ORIGINAL PAPER

Evolution of initial discontinuity for the defocusing complex modified KdV equation

Liang-Qian Kong · Lei Wang · Deng-Shan Wang · Chao-Qing Dai · Xiao-Yong Wen · Ling Xu

Abstract The complete classification of solutions to the defocusing complex modified Korteweg-de Vries (cmKdV) equation with the step-like initial condition is given by Whitham theory. The process of studying the solution of cmKdV equation can be reduced to explore four quasi-linear equations, which predicts the evolution of dispersive shock wave. The results obtained here are quite different from the defocusing nonlinear Schrödinger equation: the bidirectionality of defocusing nonlinear Schrödinger equation determines that there are two basic rarefaction and shock structures while in the cmKdV case three basic rarefaction structures and four basic dispersive shock structures are constructed which lead to more complicated classification of step-like initial condition, and wave patterns even consisted of six different regions while each of wave patterns is consisted of five regions in the defocusing nonlinear Schrödinger equation. Direct numerical simulations of cmKdV equation are agreed well with the solutions corresponding to Whitham theory.

These authors are contributed equally to this work.

L.-Q. Kong · L. Wang
Department of Mathematics and Physics, North China
Electric Power University, Beijing 102206, China

D.-S. Wang (✉) · X.-Y. Wen · L. Xu
School of Science, Beijing Information Science
and Technology University, Beijing 100192, China
e-mail: dswang@bistu.edu.cn

C.-Q. Dai
School of Sciences, Zhejiang Agriculture and Forestry
University, Hangzhou 311300, Zhejiang, China

1 Introduction

The Whitham theory was first formulated by G.B. Whitham in his seminal publication [1] in which he gave the Whitham modulation equations based on the averaged conservation laws to describe some physical phenomena such as undular bore in water and formed the basis of impressive development of dispersive hydrodynamics. The first application of Whitham theory to Korteweg-de Vries (KdV) equation was achieved by Gurevich and Pitaevskii [2] who studied the self-similar solutions for dispersive shock wave (DSW), called collisionless shock in [2], whose evolution can be described by the diagonal Whitham equation. One of its edge appears to be a soliton wave, and the harmonic wave for its opposite. The simplest expanding oscillating structure described by a Jacobian elliptic function was obtained with a step-like initial jump known as Riemann problem in [2]. Another analytical description of DSW that transformed the Whitham equation to Euler–Poisson–Darboux equation for KdV equation and nonlinear Schrödinger (NLS) equation has been presented in Refs. [3–7]. Different from the approaches in soliton theory [8–17], the Whitham theory is an efficient way to investigate the DSWs and rarefaction wave (RW) of nonlinear systems with discontinuous initial data.

From other perspective of studying DSW, the development of the inverse scattering technique [18] or Riemann-Hilbert problem [19–22] for investigating integrable systems has received lots of results. Particularly, the nonlinear steepest descent method proposed by Deift and Zhou [23] allows one to get the full asymptotic expansions of the solutions of integrable systems in various asymptotic limits. The Whitham theory is closely related to the nonlinear steepest descent method when studying the Cauchy problems of integrable systems [24].

The Riemann problem has been discussed in various important physical fields [25–31]. In photon fluid, all the possible wave patterns propagating in the normal fiber have been discussed with account of steepening effects [25]. Ref. [26] gives the classification of possible flows in two-component Bose–Einstein condensate, and the solutions of Riemann problem for Gardner equation (related to modified KdV equation) are completely classified in [27] which appear some new structures and more complicated cases compared to the KdV case. This can also be found in the case of defocusing complex modified KdV (cmKdV) equation with step-like initial data for one variable of dispersionless limit form (another one to be a constant) [28]. However, the works for both of them to be step-like in cmKdV equation are even more complicated.

Here we analyze the self-similar solutions of cmKdV equation by the cmKdV–Whitham equation with step-like initial condition except the region of genus-2. We study the solutions from a single RW and a single dispersive shock wave which we call it basic structures below, and the basic types of RW and DSW are more than defocusing NLS equation. The critical condition we will analyze in Sect. 2.1 plays an important role in distinguishing RW or DSW solutions. The complete classification of solutions to the defocusing cmKdV equation is given, which needs to be more detailed classification than defocusing NLS equation. All of the solutions we present here are compared with direct numerical solution, which have excellent agreement.

We are interested in how does the defocusing cmKdV evolve from the step-like initial data

$$q_t - 6|q|^2 q_x + \epsilon^2 q_{xxx} = 0, \qquad (1)$$

where q represents the complex wave envelope and ϵ is a small modulation scale. The Whitham equations for

cmKdV are neither strictly hyperbolic nor genuinely nonlinear systems [28]. In the past year, self-similar solutions in such kind of systems have been found and discussed in KdV hierarchy [35], mKdV [27], Landau–Lifshitz equation [26], etc.

Utilizing madelung transformation

$$q(x, t) = \sqrt{\rho} e^{i\phi/\epsilon}, \phi_x = v, \qquad (2)$$

the hydrodynamic system can be found by plugging (2) into Eq. (1)

$$\begin{cases} \rho_t - (3\rho^2 + 3v^2\rho)_x = -\epsilon^2[4\rho^{3/4}(\rho^{1/4})_{xx}]_x \\ v_t - (6\rho v + v^3)_x = -\epsilon^2[3v\rho_{xx}/2\rho - 3v(\rho_x)^2/4\rho^2 \\ \qquad\qquad + 3v_x\rho_x/2\rho + v_{xx}]_x, \end{cases} \qquad (3)$$

where ρ and v, analogs of density and velocity of the hydrodynamics, are all real functions and have the step-like initial data (7). System (3) suffices to give the solutions as $\epsilon \to 0$ until it develops a shock formed at once when muti-value region appears. After the moment when muti-value region appears, these limits can be expressed into genus-1 cmKdV–Whitham modulation equation obtained via some manipulations by the method of finite-gap integration [36]

$$\frac{\partial \lambda_i}{\partial t} + v_i(\lambda_1, \lambda_2, \lambda_3, \lambda_4)\frac{\partial \lambda_i}{\partial x} = 0, \quad i = 1, 2, 3, 4, \quad (4)$$

where

$$v_i = V + (s + 2\lambda_i)(\partial \ln L/\partial \lambda_i)^{-1},$$
$$s = \sum_{j=1}^{4} \lambda_j, \ i = 1, 2, 3, 4, \qquad (5)$$

with four slowly varying variables $\lambda_1 > \lambda_2 > \lambda_3 > \lambda_4$. Here $L = \epsilon K(m)/\sqrt{(\lambda_1 - \lambda_3)(\lambda_2 - \lambda_4)}$, $K(m)$ is the complete elliptic integrals of the first kind, the modulus $m = [(\lambda_1 - \lambda_2)(\lambda_3 - \lambda_4)]/[(\lambda_1 - \lambda_3)(\lambda_2 - \lambda_4)]$ and $V = 2\sum_{i<j} \lambda_i\lambda_j - \frac{3}{2}(\sum_{j=1}^{4} \lambda_j)^2$. The Whitham system can also be derived from the method of multiple scales expansion regardless of the integrability of the systems [30–32,34]. The boundaries connecting genus-1 and genus-0 region included in system (4) are exactly the same with the diagonal Riemann form of dispersionless limit of system (3). The periodic solution of cmKdV can be expressed as

$$\rho = \frac{1}{4}(\lambda_1 - \lambda_2 - \lambda_3 + \lambda_4)^2 + (\lambda_1 - \lambda_2)(\lambda_3 - \lambda_4)sn^2$$
$$\times \left(\frac{\sqrt{(\lambda_1 - \lambda_3)(\lambda_2 - \lambda_4)}}{\epsilon}(\xi - \xi_0), m \right), \qquad (6)$$

where sn is the Jacobian elliptic function and ξ_0 is the phase shift which is actually equal to zero in this paper [28]. But we choose ξ_0 here so that the deviation arising due to the procedure in numerical simulation from $\rho = const$ increases to wave crest can be eliminated. The procedure which is not be considered in the Whitham theory will be vanished as $\epsilon \to 0$ theoretically.

This paper is constructed as follows. In Sect. 2, we will give the self-similar solutions of basic structures which are components of general cmKdV solutions with initial conditions (7). In Sect. 3, we will solve the Whitham equation obtained in Sect. 2 numerically and make the whole classification under step-like initial conditions. Some typical scenarios have been compared to direct numerical simulation of cmKdV with remarkable agreement. We conclude this paper in Sect. 4.

2 Basic structure

In this paper, we are interested in the solution (2) of Eq. (1) whose initial data have a discontinuity at origin for both its intensity and wave number

$$\rho(x, 0) = \begin{cases} \rho_r, & x > 0 \\ 1, & x < 0 \end{cases} \quad \text{and} \quad v(x, 0) = \begin{cases} v_r, & x > 0 \\ 0, & x < 0, \end{cases} \tag{7}$$

since it gives the foundation for the more complicated scenarios. We find that the structures of the solutions evolving from (7) are so complicated that we shall investigate basic structures which are the components of the wave patterns first.

2.1 Rarefaction wave

The rarefaction wave (RW) can be solved by the dispersionless limit of Eq. (3) as $\epsilon \to 0$ due to the property of smoothness. The systems governing the rarefaction wave satisfy the non-strictly hyperbolic system

$$\begin{cases} \rho_t - (3\rho^2 + 3v^2\rho)_x = 0 \\ v_t - (6\rho v + v^3)_x = 0. \end{cases} \tag{8}$$

This limit provides the solution correct up to the moment of wave breaking, and the system can be transformed into the diagonal form

$$\frac{\partial r^{\pm}}{\partial t} + V_{\pm}(r^+, r^-)\frac{\partial r^{\pm}}{\partial x} = 0, \tag{9}$$

where we have introduced the Riemann invariants

$$r^+ = \frac{v}{2} + \sqrt{\rho}, \quad r^- = \frac{v}{2} - \sqrt{\rho}. \tag{10}$$

So we transform the initial value problem (7) from physical variables to the Riemann invariants form by means of the transformation (10)

$$r^+(x, 0) = \begin{cases} r_r^+, & x > 0 \\ 1, & x < 0 \end{cases} \quad \text{and} \quad r^-(x, 0) = \begin{cases} r_r^-, & x > 0 \\ -1, & x < 0. \end{cases} \tag{11}$$

The Riemann velocities in terms of the Riemann invariants can be expressed as

$$V_+ = -\left[\frac{15}{2}(r^+)^2 + 3r^+r^- + \frac{3}{2}(r^-)^2 \right],$$
$$V_- = -\left[\frac{15}{2}(r^-)^2 + 3r^+r^- + \frac{3}{2}(r^+)^2 \right]. \tag{12}$$

The initial condition determines that the systems (9) have the self-similar solution depending on the variable $\tau = x/t$, then we have

$$(V_+ - \tau)\frac{dr^+}{d\tau} = 0, \quad (V_- - \tau)\frac{dr^-}{d\tau} = 0. \tag{13}$$

The bidirectionality of defocusing NLS determines that there are two basic rarefaction structures to defocusing NLS [37], either r^+ or r^- to be constant. However, the characteristic of cmKdV propagates along single direction which divides the basic rarefaction structures into three types under condition (11). The solutions of (9) first type can be easily derived as

$$r^+ = r_0^+ = const, \quad r^-$$
$$= -\frac{1}{5}r_0^+ - \frac{1}{15}\sqrt{-36(r_0^+)^2 - 30 \cdot \frac{x}{t}}, \tag{14}$$

with the characteristic velocity $V_- = V_-(r_0^+, r^-)$. The second case

$$r^+ = -\frac{1}{5}r_0^- + \frac{1}{15}\sqrt{-36(r_0^-)^2 - 30 \cdot \frac{x}{t}}, \quad r^-$$
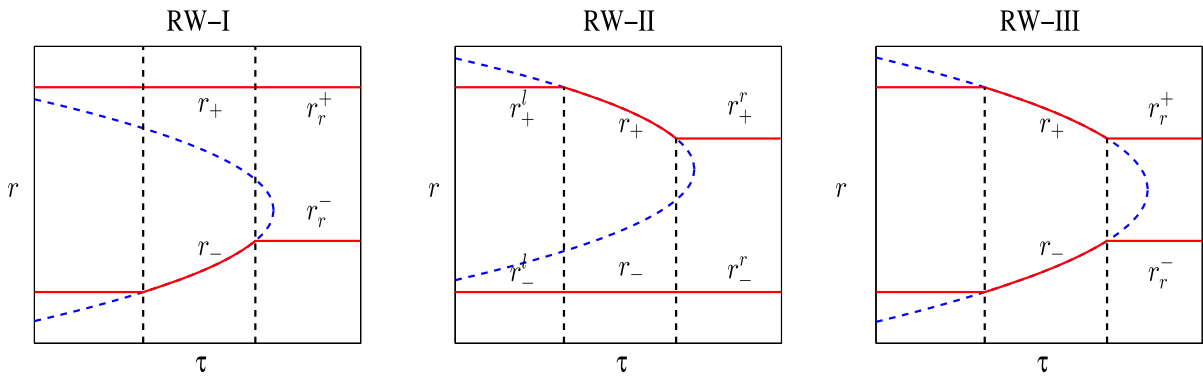$$= r_0^- = const, \tag{15}$$

Fig. 1 (Color online) Sketches of Riemann invariants of three basic RWs

with the velocity $V_+ = V_+(r^+, r_0^-)$. The third case with the meaningful solution

$$r^+ = \frac{1}{\sqrt{6}}\sqrt{-\frac{x}{t}}, r^- = -\frac{1}{\sqrt{6}}\sqrt{-\frac{x}{t}},\qquad(16)$$

with the velocity $V_+ = V_+(r^+, r^-)$. It is clear that evolution of Riemman invariants of any choice for RW will be on the parabola $\frac{15}{2}r^2 + 3r(r_0) + \frac{3}{2}(r_0)^2 + \tau = 0$ for (14) and (15) or $6r^2 + \tau = 0$ for (16) plotted in blue dashed line in Fig. 1. As we shall see, there will be the case when two Riemann invariants change simultaneously at the same spatial space which result from the property of complex modified KdV equation, i.e., not genuinely nonlinear [28], while this won't be appear in the NLS. The pure rarefaction or the plateau, exclude any type of dispersive shock wave, will occur in the situations $1 \geqslant r_r^+ \geqslant r^* \geqslant r_r^- \geqslant -1$ where $r^* = -r_0^{\pm}/5$ represents the point in which $\partial V_{\pm}/\partial r^{\pm}$ change. Otherwise the oscillating region will appear which will be discussed in Sect. 2.2. The three basic structures of Riemann invariants distributions of RWs are shown in Fig. 1. We may denote them as {RW − I} − {RW − III}. Note that formation of the third type degenerates to linearity.

2.2 Dispersive shock wave

As followed from the analysis in Sect. 2.1, the rarefaction wave solutions is valid under condition $1 \geqslant r_r^+ \geqslant r^* \geqslant r_r^- \geqslant -1$. Outside the condition, one of the Riemann invariants in (9) develops into three branches governed by the averaging mKdV–Whitham Eqs. (4) and (5). For the case of self-similar solution, the regions for DSW or RW can be determined once we give the initial data. In this subsection, six basic DSW structures that may appear evolving from the initial data (11) in Eq. (1) will be listed.

Let us recall the basic DSW structures that part of them have been proved rigorously in Ref. [28]. The first two types and the third two types of DSWs in Fig. 2 are similar to NLS case in which three of the Riemann invariants are constant and another one changes, either λ_2 or λ_3. The second two types in Fig. 2 of DSW giving rise to the not genuine nonlinear system (4) satisfy the solution in which two of the Riemann invariants are constant and the other two change. We may denote them as {DSW − I}, . . . , {DSW − VI}. The two dashed lines in Fig. 2 represent two distinct speeds characterized the DSW which is known as leading and trailing speed. The leading and trailing speed of two edges are found from Eq. (5) by the limitation $m \to 1$, when $\lambda_3 = \lambda_2$, and $m \to 0$, when $\lambda_3 = \lambda_4$ or $\lambda_2 = \lambda_1$, respectively. Note that the distributions of Riemann invariants are obtained numerically [33,34] via the scheme of two-step variant of Lax–Wendroff with nonlinear filter for the step-like function [38].

One may note that {DSW − I} and {DSW − II} are very similar to defocusing NLS case. And the reason of appearing {DSW − III} and {DSW − IV} are the same as those for {RW − III}. {DSW − V} and {DSW − VI} are the extension of {DSW − III} and {DSW − IV}. If we adjust the r_r^+ to be larger in {DSW − III} or to be smaller in {DSW − IV}, {DSW − V} and {DSW − VI} will appear naturally.

It is their appearance that makes the solution of defocusing cmKdV so complicated. It's obvious to find that {DSW − I} and {DSW − II} are symmetric with respect
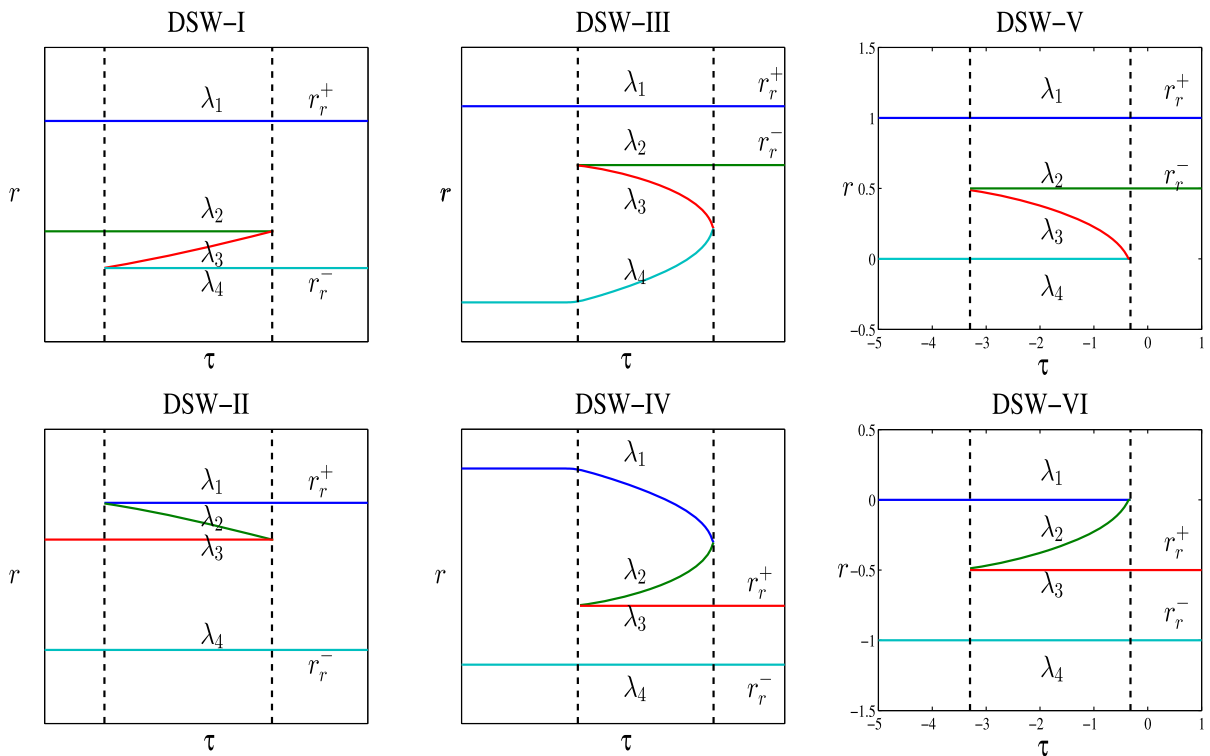
Fig. 2 (Color online) Sketches of Riemann invariants of six basic DSWs

to x axis which results in the same speed from Whitham velocity [see (22)]. So we only give two of its solutions and boundary speeds. For {DSW − I}, we have from Eq. (5)

$$\frac{x}{t} = v_3(1, -1, \lambda_3, r_r^-),$$
$$v|_{\text{left}} = v_3|_{\lambda_3=\lambda_4}, \quad v|_{\text{right}} = v_3|_{\lambda_3=\lambda_2}. \tag{17}$$

For {DSW − III}

$$\frac{x}{t} = v_3(1, r_r^-, \lambda_3, \lambda_4), \quad \frac{x}{t} = v_4(1, r_r^-, \lambda_3, \lambda_4),$$
$$v|_{\text{left}} = v_3|_{\lambda_3=\lambda_2}, \quad v|_{\text{right}} = v_3|_{\lambda_3=\lambda_4}. \tag{18}$$

In fact, due to the given initial value on the left side of this paper, {DSW − V} and {DSW − VI} will not appear separately. So we temporarily modify the initial value on the left to illustrate this type of solution.

For {DSW − V}

$$\frac{x}{t} = v_3(1, r_r^-, \lambda_3, 0),$$
$$v|_{\text{left}} = v_3|_{\lambda_3=\lambda_2}, \quad v|_{\text{right}} = v_3|_{\lambda_3=\lambda_4}. \tag{19}$$

All of the cases are obviously the extension of rarefaction waves solutions. The vertex of parabola where the sign of $\partial v/\partial r$ changes plays an important

role in distinguishing {DSW − I} − {DSW − II} and {DSW − III} − {DSW − IV}. The vertex connecting the two Riemann invariants can be determined by the formulas (20) or (21).

3 Classification of step-like initial condition

As is known to all, the self-similar solution of defocusing NLS equation with the step-like initial condition is divided into six categories. However, the solutions of defocusing cmKdV equation almost need to be divided again under each categories. Due to the diverse basic structure, the types of defocusing cmKdV solutions are more abundant than defocusing NLS case. One wave pattern is even consisted of six different regions while in the defocusing NLS case, each of wave patterns is composed of five regions.

Here, the initial condition of any basic structures discussed before have the common feature that one of the initial condition is to be constant, i.e., either $r_+|_{\text{left}} = r_+|_{\text{right}}$ or $r_-|_{\text{left}} = r_-|_{\text{right}}$. In fact, a combination of a RW and a DSW solution can also be obtained

Fig. 3 (Color online)
Example of self-similar
solution of Eq. (1). The
initial condition is given by
$r_r^+ = 0.8, r_r^- = 0.5$. **a**
Distributions of Riemann
invariants; **b** Comparison of
numerical simulation and
Whitham theory solution of
Eq. (1) with time $t = 1$ and
$\epsilon = 0.1$
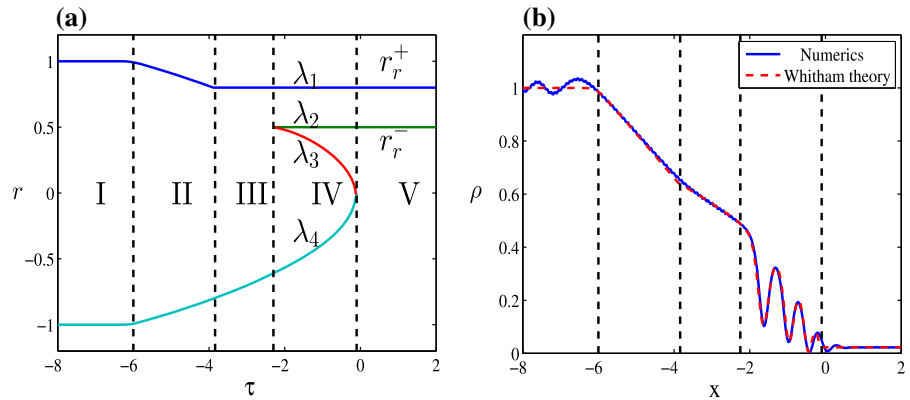
by setting one of them to be constant. We do not dis-
play it in Sect. 2 as one of the basic structure of cmKdV
equation, since it can be interpreted as the combination
solutions. Let us now discuss the initial conditions con-
sisting of four different values.

3.1 (A): $1 > r_r^+ > r_r^- > -1$

Three scenarios will appear under condition (A). We
start with condition $(A.1)$ where two RWs and a DSW
are produced.

$(A.1): 1 > r_r^+ > r_r^- > -1, r_r^- > r_{A1}^*,$

where r_{A1}^* satisfies

$$\frac{\partial v_3(r_r^+, r_r^-, r_{A1}^*, r_{A1}^*)}{\partial r_{A1}^*} = 0. \tag{20}$$

We note that if we put $r_r^- = r_{A1}^*$ into (20) we have $r_{A1}^* = -r_r^+/5$ which is the critical condition we have obtained
from Sect. 2.1, and $1 > r_r^+$ locates in the upper part of
parabola developing a rarefaction wave. We shall give
the solutions for specific regions under this condition
$(A.1)$ in details. In case of $(A.1)$, the solutions of Eq. (1)
divided into five regions are expressed as below: (see
Fig. 3)

(I) For $x/t \leqslant v_1(1, r_r^-, r_r^-, -1)$:

$r^+ = 1, r^- = -1.$

(II) For $v_1(1, r_r^-, r_r^-, -1) < x/t < v_1(r_r^+, r_r^-, r_r^-, -r_r^+)$:

$$r^+ = \frac{1}{\sqrt{6}}\sqrt{-\frac{x}{t}}, r^- = -\frac{1}{\sqrt{6}}\sqrt{-\frac{x}{t}}.$$

(III) For $v_1(r_r^+, r_r^-, r_r^-, -r_r^+) \leqslant x/t \leqslant v_3(r_r^+, r_r^-, r_r^-, r_{A1}^{**})$:

$$r^+ = r_r^+, r^- = -\frac{1}{5}r_r^+ - \frac{1}{15}\sqrt{-36(r_r^+)^2 - 30 \cdot \frac{x}{t}},$$

where r_{A1}^{**} satisfies $v_3(r_r^+, r_r^-, r_r^-, r_{A1}^{**}) = v_4(r_r^+, r_r^-, r_r^-, r_{A1}^{**})$ located in the interval $(-1, r_{A1}^*)$.

(IV) For $v_3(r_r^+, r_r^-, r_r^-, r_{A1}^{**}) < x/t < v_3(r_r^+, r_r^-, r_{A1}^*, r_{A1}^*)$:

$$\lambda_1 = r_r^+, \lambda_2 = r_r^-, \frac{x}{t} = v_3(r_r^+, r_r^-, \lambda_3, \lambda_4),$$

$$\frac{x}{t} = v_4(r_r^+, r_r^-, \lambda_3, \lambda_4).$$

(V) For $x/t \geqslant v_3(r_r^+, r_r^-, r_{A1}^*, r_{A1}^*)$:

$$r^+ = r_r^+, r^- = r_r^-.$$

So the solutions are composed of plateau, {RW −
III}, {RW − I}, {DSW − III} and a plateau, respec-
tively.

The boundary velocities of DSW $x/t = v_3(r_r^+, r_r^-, r_r^-, r_{A1}^{**})$ and $x/t = v_3(r_r^+, r_r^-, r_{A1}^*, r_{A1}^*)$ are known
as leading edge and trailing edge, respectively. The
regions that outside the boundaries of DSW (genus-
1) are controlled by rarefaction waves (9). The Rie-
mann invariants matching of the zero-phase region and
single-phase region are given as follows: At trailing
edge where $\lambda_3 = \lambda_4$, $(\lambda_1, \lambda_2) =$ the rarefaction wave
solution outside the oscillation region; at leading edge
where $\lambda_3 = \lambda_2$, $(\lambda_1, \lambda_4) =$ the rarefaction wave solu-
tion outside the oscillation region. For simplicity, we
do not show Roman number in each region in the fol-
lowing content.

Now it's natural to consider the condition

$(A.2): 1 > r_r^+ > r_r^- > -1, r_r^+ < r_{A2}^*,$

where r_{A2}^* satisfies

Fig. 4 (Color online) Same as Fig. 3 except $r_r^+ = 0.5, r_r^- = -0.1$
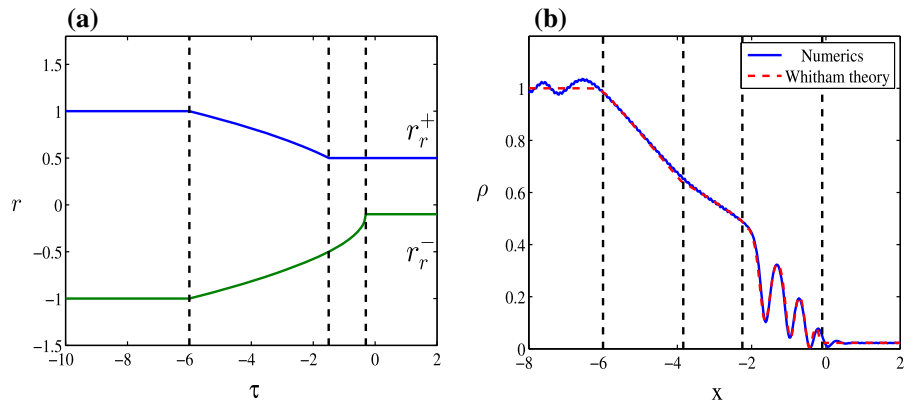
$$\frac{\partial v_2(r_{A2}^*, r_{A2}^*, r_r^+, r_r^-)}{\partial r_{A2}^*} = 0. \tag{21}$$

The critical condition can also be obtained if we put $r_r^+ = r_{A2}^*$ into (21), then we have $r_{A2}^* = -r_r^-/5$. The results of Riemann distribution under $(A.2)$ and $(A.1)$ are symmetric with respect to x-axis, i.e., $\lambda_i^{'} = -\lambda_{5-i}, i = 1...4$, so the density ρ under condition $(A.1)$ and $(A.2)$ for each regions are exactly the same (see [6]). From (5), we have

$$\begin{aligned} v_j(\lambda_1^{'}, \lambda_2^{'}, \lambda_3^{'}, \lambda_4^{'}) &= V + (s + 2\lambda_j)(\partial \ln L/\partial \lambda_j)^{-1} \\ &= V + (-s - 2\lambda_i)(-\partial \ln L/\partial \lambda_i)^{-1} \\ &= V + (s + 2\lambda_i)(\partial \ln L/\partial \lambda_i)^{-1} \\ &= v_i(\lambda_1, \lambda_2, \lambda_3, \lambda_4), \quad j = 5 - i, \end{aligned} \tag{22}$$

which means that the boundaries for each region under $(A.2)$ are the same as those which are under $(A.1)$.

In both $(A.1)$ and $(A.2)$, which we have discussed before, shock waves are produced. Then we shall discuss final cases under that only rarefaction wave produced under the condition $1 > r_r^+ > r_r^- > -1$.

$(A.3) : 1 > r_r^+ > r_r^- > -1, r_r^+ \geqslant r_{A2}^*, r_r^- \leqslant r_{A1}^*$

The solutions evolving from condition $(A.3)$ are all the combination of RWs which is easier to analysis than before. Condition $(A.3)$ only gives three possible Riemann distributions: $(A.31)$: $r_r^+ > -r_r^-$; $(A.32)$: $r_r^+ = -r_r^-$; $(A.33)$: $r_r^+ < -r_r^-$. Indeed, the density of $(A.31)$ and $(A.33)$ is the same due to the symmetric of their Riemann distributions. $(A.32)$ is actually the case of $\{RW - III\}$. So we only list the case $(A.31)$ as an example in Fig. 4. In Fig. 4, the wave consists of $\{RW-III\}$ and $\{RW-I\}$ whose solutions and velocities

have been given in Sect. 2.1, so we here neglect the detailed description to Fig. 4.

3.2 $(B) : 1 > r_r^+ \geqslant -1 > r_r^-$

Two scenarios will appear under condition (B): $(B.1)$: $r_r^+ \geqslant r_B^*$; $(B.2)$: $r_r^+ < r_B^*$, where r_B^* satisfies $\partial v_1(r_B^*, r_B^*, r_r^+, r_r^-)/\partial r_B^* = 0$. In $(B.1)$, a DSW and a rarefaction are produced which also appear in NLS case [37]. So we only give the discussion under the condition $(B.2)$ here.

$(B.21) : 1 > r_r^+ \geqslant -1 > r_r^-, r_r^+ < r_B^*, r_r^+ > r_B^{**}$

We notice that the choice of r_r^+ influences the leading edge speed of $\{DSW - IV\}$ which is marked as V_{DSW} in Fig. 5a, V_{RW} represents the leading speed of $\{RW - II\}$ before $\{DSW - IV\}$. Obviously, there exists a point r_B^{**} that makes the speed of $\{DSW-IV\}$ exactly the same with $\{RW - II\}$, that is

$$v_1(1, r_B^{**}, r_B^{**}, r_r^-) = v_2(1, r_B^{**}, r_B^{**}, r_r^-). \tag{23}$$

So we have $r_B^{**} = -3/2 - r_r^-/2$. We shall give the case where the propagation speed of $\{DSW - IV\}$ is slower than $\{RW - II\}$'s first.

In Fig. 5, we present the Riemann distributions under condition $(B.21)$ in (a) and the corresponding self-similar solution where two DSWs are produced for cmKdV equation in (b). The intermediate state connecting two DSWs are composed of a plateau and a rarefaction, the deviation of the plateau in (b) results from the plane oscillation during numerical simulation. The boundaries of those regions are also plotted by

Fig. 5 (Color online) Same as Fig. 3 except $r_r^+ = -0.3, r_r^- = -1.2$
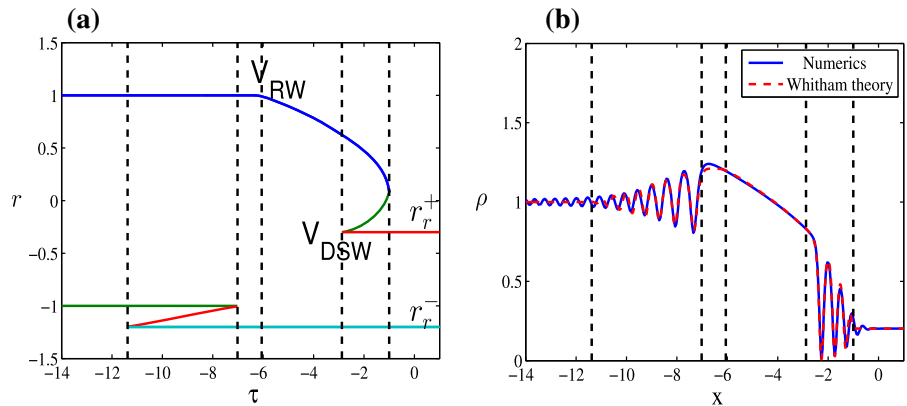
five black dashed lines in Fig. 5. The solutions of the cmKdV equation which are divided into six regions can be expressed as follows:

For $x/t \leqslant v_3(1, -1, r_r^-, r_r^-)$:

$$r^+ = 1, \ r^- = -1.$$

For $v_3(1, -1, r_r^-, r_r^-) < x/t < v_3(1, -1, -1, r_r^-)$:

$$\lambda_1 = 1, \lambda_2 = -1, x/t = v_3(1, -1, \lambda_3, r_r^-), \lambda_4 = r_r^-.$$

For $v_3(1, -1, -1, r_r^-) \leqslant x/t < v_1(1, r_r^+, r_r^+, r_r^-)$:

$$r^+ = 1, \ r^- = r_r^-.$$

For $v_1(1, r_r^+, r_r^+, r_r^-) \leqslant x/t < v_1(r_B^{***}, r_r^+, r_r^+, r_r^-)$:

$$r^+ = -\frac{1}{5}r_r^- + \frac{1}{15}\sqrt{-36(r_r^-)^2 - 30 \cdot \frac{x}{t}}, \ r^- = r_r^-,$$

where r_B^{***} satisfies $v_1(r_B^{***}, r_r^+, r_r^+, r_r^-) = v_2(r_B^{***}, r_r^+, r_r^+, r_r^-)$ located in the interval $(r_B^*, 1)$.

For $v_1(r_B^{***}, r_r^+, r_r^+, r_r^-) \leqslant x/t \leqslant v_2(r_B^*, r_B^*, r_r^+, r_r^-)$:

$$x/t = v_1(\lambda_1, \lambda_2, r_r^+, r_r^-),$$
$$x/t = v_2(\lambda_1, \lambda_2, r_r^+, r_r^-), \lambda_3 = r_r^+, \lambda_4 = r_r^-.$$

For $x/t > v_2(r_B^*, r_B^*, r_r^+, r_r^-)$:

$$r^+ = r_r^+, r^- = r_r^-.$$

So the solutions are composed of plateau, {DSW − I}, plateau, {RW − II}, {DSW − IV} and a plateau, respectively.

$(B.22)$: $1 > r_r^+ \geqslant -1 > r_r^-, r_r^+ < r_B^*, r_r^+ = r_B^{**}$

As we analyzed in $(B.21)$, $r_r^+ = r_B^{**}$ means {RW − II} is covered totally by {DSW − IV} due to the same speed. In other words, the leading edge and trailing edge of the {RW − II} are the same which leads to

the region of {RW − II} disappear (see Fig. 6a). The case of $(B.22)$ and $(B.21)$ is much similar, so we do not repeat the same description of each region but only give the Riemann distribution and wave profile. In Fig. 6a, we choose $r_r^+ = r_B^{**} = -3/2 - r_r^-/2 = -0.9$. The deviation of the intermediate plateau in (b) results from the plane oscillation during numerical simulation.

$(B.23)$: $1 > r_r^+ \geqslant -1 > r_r^-, r_r^+ < r_B^*, -1 < r_r^+ < r_B^{**}$

An example of $(B.23)$ is displayed in Fig. 7a. The plateau connecting {DSW − I} and {DSW − IV} in Fig. 6a is split into a smaller plateau and a small {DSW − VI}. The solutions of cmKdV under $(B.23)$ can be expressed as follows:

For $x/t \leqslant v_3(1, -1, r_r^-, r_r^-)$:

$$r^+ = 1, \ r^- = -1.$$

For $v_3(1, -1, r_r^-, r_r^-) < x/t < v_3(1, -1, -1, r_r^-)$:

$$\lambda_1 = 1, \lambda_2 = -1, x/t = v_3(1, -1, \lambda_3, r_r^-), \lambda_4 = r_r^-.$$

For $v_3(1, -1, -1, r_r^-) \leqslant x/t < v_2(1, r_r^+, r_r^+, r_r^-)$:

$$r^+ = 1, \ r^- = r_r^-.$$

For $v_2(1, r_r^+, r_r^+, r_r^-) \leqslant x/t < v_1(1, r_B^{4*}, r_r^+, r_r^-)$:

$$\lambda_1 = 1, x/t = v_2(1, \lambda_2, r_r^+, r_r^-), \lambda_3 = r_r^+, \lambda_4 = r_r^-,$$

where r_B^{4*} satisfies $v_1(1, r_B^{4*}, r_r^+, r_r^-) = v_2(1, r_B^{4*}, r_r^+, r_r^-)$.

For $v_1(1, r_B^{4*}, r_r^+, r_r^-) \leqslant x/t \leqslant v_2(r_B^*, r_B^*, r_r^+, r_r^-)$:

$$x/t = v_1(\lambda_1, \lambda_2, r_r^+, r_r^-),$$
$$x/t = v_2(\lambda_1, \lambda_2, r_r^+, r_r^-), \lambda_3 = r_r^+, \lambda_4 = r_r^-.$$

For $x/t > v_2(r_B^*, r_B^*, r_r^+, r_r^-)$:

$$r^+ = r_r^+, r^- = r_r^-.$$

$(B.24)$: $1 > r_r^+ \geqslant -1 > r_r^-, r_r^+ < r_B^*, r_r^+ = -1$

Fig. 6 (Color online) Same as Fig. 3 except $r_r^- = -1.2, r_r^+ = -0.9$
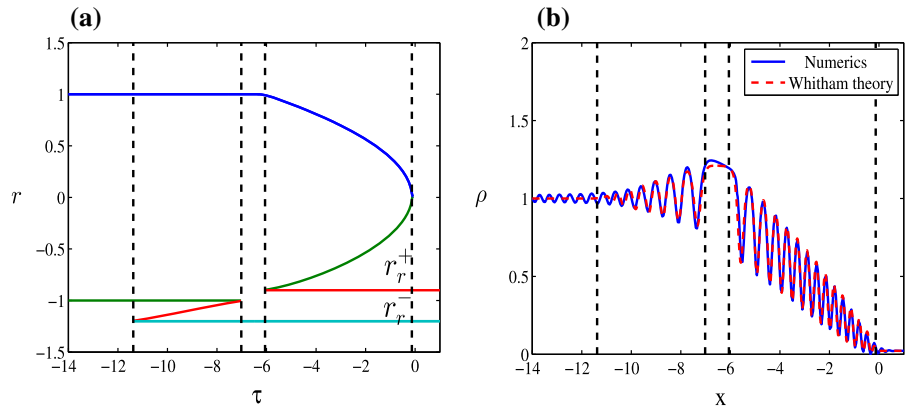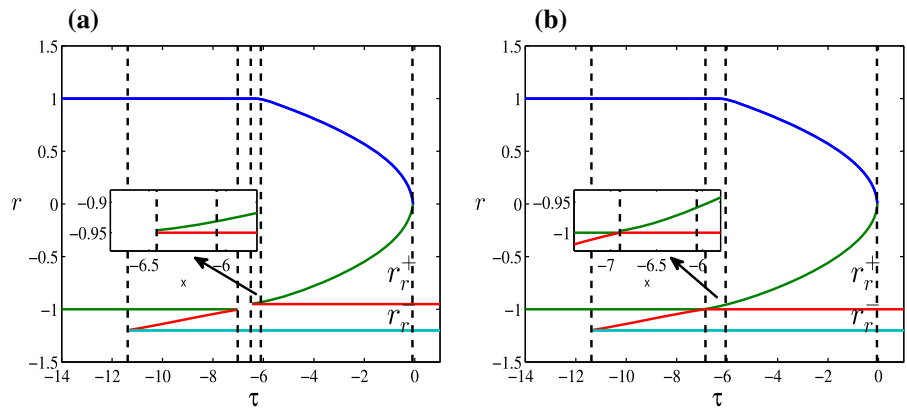

Fig. 7 (Color online) Self-similar solutions of Riemann distributions. The initial conditions are $r_r^- = -1.2 : \mathbf{a}\, r_r^+ = -0.95; \mathbf{b}\, r_r^+ = -1$

An example of (B.24) is displayed in Fig. 7b in order to make a comparison with (B.23). The plateau connecting {DSW − I} and {DSW − IV} in (a) is covered totally by a {DSW − VI} in (b). We find that $v_3(1, -1, -1, r_r^-) = v_2(1, -1, -1, r_r^-)$, so we can get the solution in this case as long as the left and right speeds of the third area in Fig. 6b to be equal. The wave profile of cmKdV under (B.24) is composed of plateau, {DSW − I}, {DSW − VI}, {DSW − IV} and plateau.

The solutions of (B.22)–(B.24) are much similar, and the only difference between them is the changes of intermediate plateau. So we only present the Riemann distributions under condition (B.23) and (B.24).

3.3 (C) : $r_r^+ > 1 > -1 > r_r^-$

The solution under (C) has three possibilities: (C.1) : $r_r^+ < -r_r^-$; (C.2) : $r_r^+ = -r_r^-$; (C.3) : $r_r^+ > -r_r^-$. Obviously, the Riemann distributions of (C.1) and (C.3) are symmetric and the formation of the profile for ρ

is the same. From the condition (C) : $r_r^+ > 1 > -1 > r_r^-$ what we see here in not self-similar case is emergence of the genus-2 regions due to the collision of two DSWs, which can't be described by the genus-1 Whitham system (4) and (6) definitely. One example corresponding to case (C.3) that the genus-2 region surrounded by two genus-1 regions is shown in Fig. 8. In Fig. 8a, we leave the blank for the region of collision (genus-2 region) where we do not study temporary. And the boundary of genus-2 region between $x = s_1 t$ and $x = s_2 t$ is plotted in dashed lines in Fig. 8a where $s_1 = v_3(1, -1, r_r^-, r_r^-) = -11.28, s_2 = v_2(r_r^+, 1, 1, -1) = -8.375$. In Fig. 8b, we present the numerical simulation under the same condition of Fig. 8a, four white lines represent the boundaries of each region corresponding to four black dotted line in Fig. 8a. From the numerical simulation, we see that amplitude of genus-2 region is oscillating for each wave crest as time increases, while for genus-1 region the amplitude is invariable.

Fig. 8 (Color online) The initial conditions are given by $r_r^+ = 1.5, r_r^- = -1.2$. **a** Riemann distributions under (C.3) for genus = 0 region and genus = 1 region. **b** Numerical results under (C.3). White lines represent the boundary of each region corresponding the black dashed lines in **a**
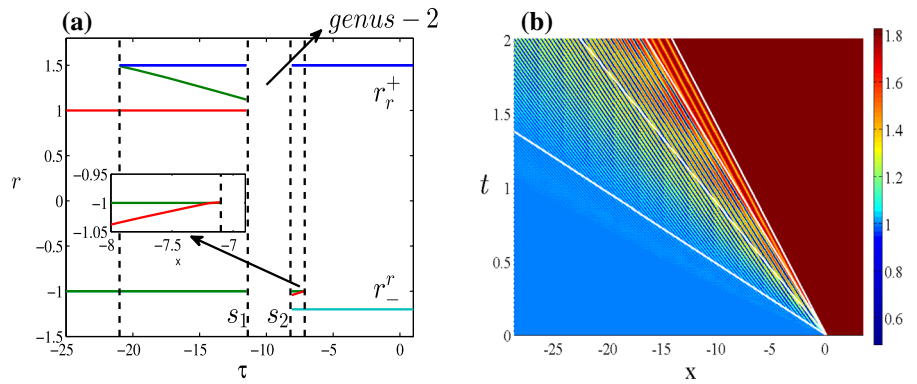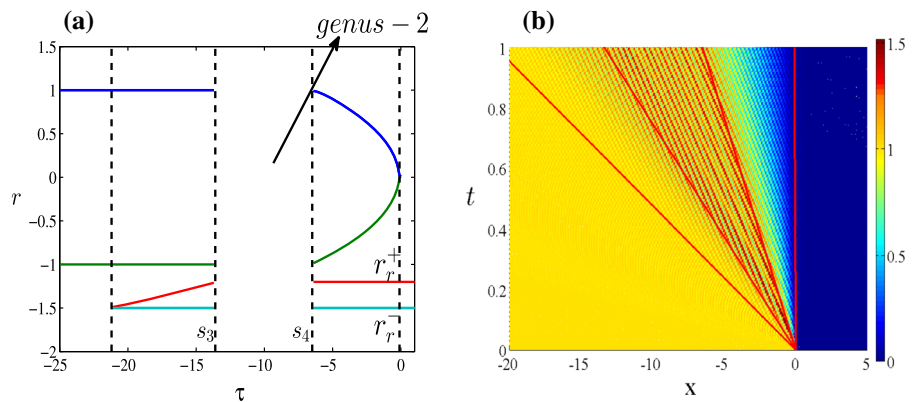

Fig. 9 (Color online) Same as Fig. 8 except $r_r^+ = -1.2, r_r^- = -1.5$

The more complicated cases that the region for genus-1 will be overlapped totally by genus-2 region under the condition (C.2) are not present here.

In fact, the boundaries of genus-2 region obtained depending on genus-1 Whitham equation are actually not precisely. The detailed discussion of the genus-2 region here is beyond the scope of this article, and we will discuss it in the future.

3.4 $(D): 1 > -1 > r_r^+ > r_r^-$

The genus-2 region also appears due to the collision of two DSWs under condition (D). Again, we do not discuss here in detail, but only give the solutions for genus-1 and genus-0. An example including the three regions has been shown in Fig. 9. In fact, the situations for (C) and (D) are the same to some extent except the type of DSWs for collision is different. The form to exhibit the solution is the same as Fig. 8. The boundaries of genus-2 region are $s_3 = v_2(1, -1, r_r^+ . r_r^-) \approx -13.4$, $s_4 = v_3(1, -1, r_r^+ . r_r^-) \approx -6.53$.

3.5 $(E): r_r^+ > r_r^- > 1 > -1, \quad (F): r_r^+ > 1 \geqslant r_r^- > -1$

The solutions under (E), (F) are the same as those which are under (D), (B). Indeed, if we set $r_{rE}^+ = -r_{rD}^-, r_{rE}^- = -r_{rD}^+$ where subscripts (D) and (E) represent the parameter under condition (D) and (E), respectively, we have at once $1 > -1 > r_{rD}^+ > r_{rD}^-$ which is exactly coincided with the condition (D). This kind of transformation do not have any effect on expression (6). The same procedure could also be applied in (F).

4 Conclusion

In this paper, the Riemann problem of the complex mKdV equation has been solved. The process of classification needs to be more detailed than the NLS case due to its property of not genuinely nonlinear, but the symmetry indeed simplifies the classification. We give the solutions for each conditions except the regions for genus-2. Some of the cases have been compared with

the direct numerical simulation, which exhibits remarkable agreement.

Compliance with ethical standards

Conflict of Interest We declare that we do not have any commercial or associative interest that represents a conflict of interest in connection with the paper submitted.

References

1. Whitham, G.B.: Nonlinear dispersive waves. Proc. R. Soc. Lond. Ser. A **283**, 238 (1965)
2. Gurevich, A.V., Pitaevskii, L.P.: Nonstationary structure of a collisionless shock wave. Sov. Phys. JETP **2**, 291 (1974)
3. Gurevich, A.V., Krylov, A.L., EL, G.A.: Evolution of a Riemann wave in dispersive hydrodynamics. Sov. Phys. JETP **74**, 957 (1992)
4. Wright, O.C.: Korteweg-de Vries zero dispersion limit: through first breaking for cubic-like analytic initial data. Commmun. Pure Appl. Math. **46**, 423 (1993)
5. Tian, F.R., Ye, J.: On the Whitham equations for the semiclassical limit of the defocusing nonlinear Schrödinger equation. Commmun. Pure Appl. Math. **52**, 655 (1999)
6. Tian, F.R.: Oscillations of the zero dispersion limit of the Korteweg-de Vries equation. Commmun. Pure Appl. Math. **46**, 1093 (1993)
7. Tian, F.R.: The Whitham-type equations and linear overdetermined systems of Euler–Poisson–Darboux type. Duke Math. J. **74**, 203 (1994)
8. Ma, W.X., Zhou, Y.: Lump solutions to nonlinear partial differential equations via Hirota bilinear forms. J. Differ. Equ. **264**(4), 2633 (2018)
9. Zhang, J.B., Ma, W.X.: Mixed lump-kink solutions to the BKP equation. Comput. Math. Appl. **74**, 591 (2017)
10. McAnally, M., Ma, W.X.: An integrable generalization of the D-Kaup–Newell soliton hierarchy and its bi-Hamiltonian reduced hierarchy. Appl. Math. Comput. **323**, 220 (2018)
11. Dong, H.H., Zhao, K., Yang, H.Q., Li, Y.Q.: Generalised $(2 + 1)$-dimensional super MKdV hierarchy for integrable systems in soliton theory. East Asian J. Appl. Math. **5**, 256 (2015)
12. Manukure, S., Zhou, Y., Ma, W.X.: Lump solutions to a $(2 + 1)$-dimensional extended KP equation. Comput. Math. Appl. **75**, 2414 (2018)
13. Ma, W.X.: Abundant lumps and their interaction solutions of $(3 + 1)$-dimensional linear PDEs. J. Geom. Phys. **133**, 10 (2018)
14. Xu, X.X., Sun, Y.P.: Two symmetry constraints for a generalized Dirac integrable hierarchy. J. Math. Analy. Appl. **458**, 1073 (2018)
15. Zhao, H.Q., Ma, W.X.: Mixed lump–kink solutions to the KP equation. Comput. Math. Appl. **74**, 1399 (2017)
16. Ma, W.X., Yong, X.L., Zhang, H.Q.: Diversity of interaction solutions to the $(2 + 1)$-dimensional Ito equation. Comput. Math. Appl. **75**, 289 (2018)
17. Wang, D.S., Liu, J.: Integrability aspects of some two-component KdV systems. Appl. Math. Lett. **79**, 211 (2018)
18. Lax, P., Levermorem, C.: The small dispersion limit of the Korteweg-de Vries equation. Commun. Pure Appl. Math. **36**, 253 (1983)
19. Buckingham, R., Venakides, S.: Long-time asymptotics of the nonlinear Schrödinger equation shock problem. Commun. Pure Appl. Math. **60**, 1349 (2007)
20. Wang, D.S., Wang, X.L.: Long-time asymptotics and the bright N-soliton solutions of the Kundu–Eckhaus equation via the Riemann–Hilbert approach. Nonlinear Anal. Real World Appl. **41**, 334 (2018)
21. Wang, D.S., Guo, B.L., Wang, X.L.: Long-time asymptotics of the focusing Kundu–Eckhaus equation with nonzero boundary conditions. J. Differ. Equ. **266**, 5209 (2019)
22. Zhang, X.E., Chen, Y.: Inverse scattering transformation for generalized nonlinear Schrödinger equation. Appl. Math. Lett. **98**, 306 (2019)
23. Deift, P., Zhou, X.: A steepest descent method for oscillatory Riemann–Hilbert problems. Asymptotics for the MKdV equation. Ann. Math. **137**, 295 (1993)
24. Jenkins, R.: Regularization of a sharp shock by the defocusing nonlinear Schrödinger equation. Nonlinearity **28**, 2131 (2015)
25. Ivanov, S.K., Kamchatnov, A.M.: Riemann problem for the photon fluid: self-steepening effects. Phys. Rev. A **96**, 053844 (2017)
26. Ivanov, S.K., Kamchatnov, A.M., Congy, T., Pavloff, N.: Solution of the Riemann problem for polarization waves in a two-component Bose–Einstein condensate. Phys. Rev. E **96**, 062202 (2017)
27. Kamchatnov, A.M., Kuo, Y.H., Lin, T.C., Horng, T.L., Gou, S.C., Clift, R., El, G.A., Grimshaw, R.H.: Undular bore theory for the Gardner equation. Phys. Rev. E **86**, 036605 (2012)
28. Kodama, Y., Pierce, V.U., Tian, F.R.: On the Whitham equations for the defocusing complex modified KdV equation. SIAM J. Math. Anal. **41**, 26 (2008)
29. El, G.A., Nguyen, L.T.K., Smyth, N.: Dispersive shock waves in systems with nonlocal dispersion of Benjamin–Ono type. Nonlinearity **31**, 1392 (2018)
30. Ablowitz, M.J., Biondini, G., Wang, Q.: Whitham modulation theory for the Kadomtsev–Petviashvili equation. Proc. R. Soc. A **473**, 20160695 (2017)
31. Ablowitz, M.J., Biondini, G., Rumanov, I.: Whitham modulation theory for $(2 + 1)$-dimensional equations of Kadomtsev–Petviashvili type. J. Phys. A **51**, 215501 (2018)
32. Ablowitz, M.J., Biondini, G., Wang, Q.: Whitham modulation theory for the two-dimensional Benjamin–Ono equation. Phy. Rev. E **96**, 032225 (2017)
33. Grava, T., Klein, C.: Numerical solution of the small dispersion limit of Korteweg de Vries and Whitham equations. Commun. Pure Appl. Math. **60**, 1623 (2007)
34. Ablowitz, M.J., Demirci, A., Ma, Y.P.: Dispersive shock waves in the Kadomtsev–Petviashvili and two dimensional Benjamin–Ono equations. Physica D **333**, 84 (2016)

35. Pierce, V.U., Tian, F.R.: Self-similar solutions of the non-strictly hyperbolic Whitham equations for the KdV hierarchy. Dyn. Partial Differ. Equ. **4**, 263 (2007)

36. Kamchatnov, A.M.: New approach to periodic solutions of integrable equations and nonlinear theory of modulational instability. Phys. Rep. **286**, 199 (1997)

37. El, G.A., Geogjaev, V.V., Gurevich, A.V., Krylov, A.L.: Decay of an initial discontinuity in the defocusing NLS hydrodynamics. Physica D **86**, 186 (1995)

38. Engquist, B., Lötstedt, P., Sjögreen, B.: Nonlinear filters for efficient shock computation. Math. Comput. **52**, 509 (1989)